SIMULATION OF ROUND LEADING EDGE AEROTHERMODYNAMICS

Wilson F. N. Santos
National Institute for Space Research
Combustion and Propulsion Laboratory
12630-000 Cachoeira Paulista, SP, Brazil
wilson@lcp.inpe.br

Abstract. *Effects of incomplete surface accommodation in rarefied gas flow have been studied by using the Direct Simulation Monte Carlo (DSMC) method in conjunction with the Cercignani-Lampis-Lord gas surface interaction model. The DSMC calculations examine differences in predictions of aerodynamic forces and heat transfer between full and partial surface accommodation for hypersonic flow past round leading edges at zero incidence. The aerothermodynamic performance of the round leading edges is assessed by using the heat transfer rate, the total drag and the shock wave standoff distance. Twenty-five combinations of nose radius, normal and tangential accommodation coefficients were used in the simulation. For the flow conditions considered, the analysis showed that stagnation point heating, total drag and shock standoff distance are sensitive to changes on either the normal or tangential accommodation coefficient. The results substantiate that it becomes imperative to take surface accommodation into account in order to make accurate predictions of the aerodynamic forces on, and heat transfer rates to, bodies in rarefied hypersonic flow.*

Keywords: *hypersonic flow, rarefied flow, DSMC, round leading edge, gas-surface interaction.*

1. Introduction

Supersonic and hypersonic flight vehicles are commonly designed and manufactured with blunt noses. A large nose radius helps to withstand, distribute, and dissipate the heat and pressure loadings that are often most extreme at the vehicle bow. At one hand, for the particular case of atmospheric entry and re-entry vehicles, high bluntness contributes to the drag production that is necessary to decelerate from suborbital to subsonic speed. On the other hand, supersonic and hypersonic cruise vehicles need low drag to efficiently maintain velocity, a requirement satisfied with a small but finite nose bluntness. In this scenario, the leading edge of the vehicle is one of the key issues concerning hypersonic configurations.

Certain configurations, such as hypersonic waveriders, are designed analytically with infinitely sharp leading edges for shock wave attachment, in order to contain the high-pressure air that produces useful lifting force. Nevertheless, these leading edges must then be blunted for heat transfer and manufacturability, with associated departure from ideal performance. An ongoing in the application of hypersonic waverider shapes to the design of realistic flight systems is therefore the concern that the predicted performance of analytically derived shapes, with infinitely sharp leading edges, will not be achieve when actual leading edges are blunted for heat transfer and manufacture. In this way, it has been generally assumed that a round leading edge, with constant radius of curvature near the stagnation point, is the appropriate blunting geometry.

Recently, considerable attention (Shvets et al., 2005) has been given to the problem of calculating aerodynamic performance of hypersonic waverider vehicles for high-altitude/low-density applications. Nonetheless, in hypersonic flight at high altitudes, gas-surface interaction is the dominant physical process governing aerodynamic forces and heat transfer. The influence of the model of gas-surface interaction on the flow parameters increases substantially as the gas rarefaction increases, and a correct choice of the model for calculating hypersonic rarefied flows plays an important role.

It has been known from experimental data that one can approximate gas-surface interactions on engineering surface with contamination from air and surface roughness by using the fully diffusion reflection model. Diffuse reflection occurs in such a manner that all previous directional history is erased, and the molecules are reflected equally in all directions. However, according to molecular beam studies and direct measurements of accommodation, the diffuse reflection model is unrealistic, except for highly contaminated surface. Surfaces of vehicles at high altitude will become gradually decontaminated, and it is likely that the reduction in accommodation will have significant effects on aerodynamic forces and heat transfer rates. As a result, molecules reflected from clean surface show lobular distribution in direction, which tends to approach the specular angle for very high energy and/or low angle of attack.

Among the several phenomenological models that have been proposed to describe gas-surface interactions, that of Cercignani-Lampis-Lord (CLL) model (Lord, 1991) appears to be the most successful to handle such behavior. The CLL model incorporates independent accommodation coefficients for the normal and tangential velocity components. It produces physically realistic distributions of direction and energy or scattered molecules and provides a continuous spectrum of behavior from specular to diffuse reflection.

The study at hand investigates the differences in the aerothemodynamic quantities predicted with the CLL model, which is implemented into a DSMC code. For the idealized situation of two-dimensional rarefied hypersonic flow, calculations have been performed on round leading edges. Of particular interest are the behaviors of stagnation point heating, total drag and shock wave displacement.

2. Leading Edge Geometry Definition

The round leading edges are modeled by assuming a sharp leading edge of half angle θ with a reference circular cylinder of radius R inscribed tangent to the wedge. The round leading edges are inscribed between the wedge and the cylinder. The circular cylinder diameter provides a reference for the amount of blunting desired on the leading edges. It was assumed a leading edge half angle of 10 degree and a reference circular cylinder diameter of 10^{-2}m. In addition to the reference circular cylinder, four more circular cylinders with different nose radii were chosen for round leading edges. The dimensionless nose radius R_N/λ_∞ for the four bodies are 0.02, 0.1, 1 and 2, where λ_∞ is the freestream mean free path. Figure 1(a) illustrates the construction for the round leading edges investigated.
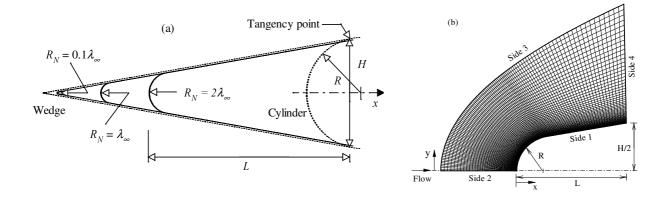

Figure 1: Drawing illustrating (a) the leading edge shapes and (b) the computational domain.

3. Computational Method and Procedure

It is well known that the Direct Simulation Monte Carlo (DSMC) method introduced by Bird (1994) has become a reliable and efficient kinetic approach for modeling rarefied gas flows. Typical applications include high altitude rockets plumes, microelectromechanical systems (MEMS) devices, spacecraft propulsion and contamination, low-pressure plasma material-processing reactors, and reentry vehicles. Although these applications encompass a wide range of spatial and temporal scales, they are united by the same underlying physics of moderate or high Knudsen number flows. The Knudsen number Kn is de ratio of the gas mean free path λ to the characteristic length scale of the problem. It is generally accepted that the rarefied transition flow regime lies in the range of $0.01 < Kn < 10$. The transition regime is the category of flow that falls between the continuum regime, where the Navier-Stokes equations are valid, and the free molecular regime, which is the limit of infinite Knudsen number.

The DSMC method employs thousands or millions representative molecules in order to reproduce the behavior of a far larger number of real molecules within the flow. The strategy of the method is to directly track the molecular trajectory and status based on the collision mechanics to model molecules in a computer and then obtain physical quantities of interest through statistical sampling.

Collisions in the present DSMC code are modeled by using the variable hard sphere (VHS) molecular model (Bird, 1981) and the no time counter (NTC) collision sampling technique (Bird, 1989). Repartition energy among internal and translational modes is controlled by the Borgnakke-Larsen statistical model (Borgnakke and Larsen, 1975). Simulations are performed using a non-reacting gas model for a constant freestream gas composition consisting of 76.3% of N_2 and 23.7% of O_2. The reasons for that are two fold: (1) the primary issue is to compare the impact of partial surface accommodation on the properties with that for diffuse reflection case already investigated as a non-reacting gas model, and (2) due to fact that, for sharp leading edges (R_N/λ_∞ of 0.02 and 0.1), vibrational modes were not so excited in order to initiate the dissociation process. Energy exchanges between the translational and internal modes, rotational and vibrational, are considered. Relaxation collision numbers of 5 and 50 were used for the calculations of rotation and vibration, respectively.

The computational domain used for the calculation is made large enough so that body disturbances do not reach the upstream and side boundaries, where freestream conditions are specified. A schematic view of the computational domain is depicted in Fig. 1(b). Side 1 is defined by the body surface. Reflection with incomplete surface accommodation is the condition applied to this side. Advantage of the flow symmetry is taken into account, and molecular simulation is applied to one-half of a full configuration. Thus, side 2 is a plane of symmetry. In such a boundary, all flow gradients normal to the plane are zero. At the molecular level, this plane is equivalent to a specular reflecting boundary. Side 3 is the freestream side through which simulated molecules enter and exit. Finally, the flow at the downstream outflow boundary, side 4, is predominantly supersonic and vacuum condition is specified (Bird, 1994). At this boundary, simulated molecules can only exit.

In order to simulate the partial surface accommodation, the CLL model (Lord, 1991) was included in this DSMC calculation. The CLL model is derived assuming that there is no coupling between the normal and tangential momentum components. The two adjustable parameters appearing in the CLL model are the normal component of translational energy α_n and the tangential component of momentum σ_t.

Usually, the two accommodation coefficients in the CLL model are expressed as being,

$$\alpha = \frac{e_i - e_r}{e_i - e_w} \qquad \sigma_t = \frac{\tau_i - \tau_r}{\tau_i} \tag{1a, 1b}$$

where terms e and τ refer to the energy flux to the surface and the momentum flux acting tangential to the surface per unit area per unit time, respectively; subscripts i and r stand for the incident and reflected components, and w refers to the component that would be produced by a diffuse reflection at the temperature of the surface.

Finally, no attempt has been made to compare the results of the present calculations with such experimental results as exist. Most of these have been obtained in wind-tunnel environments where no control of surface condition is possible and surface would be expected to be highly contaminated and to exhibit virtually complete accommodation. Moreover, the relative few experiments in which effects of partial accommodation appear have all used helium rather that air.

4. Computational Conditions

The flow conditions, summarized in Tab. 1, represent those experienced by a spacecraft at an altitude of 70 km. This altitude is associated with the transitional flow regime, which is characterized by the overall Knudsen number of the order of or larger than 10^{-2}. Referring to Tab. 1, T_∞, p_∞, ρ_∞, n_∞, μ_∞, and λ_∞ stand respectively for temperature, pressure, density, number density, viscosity and mean free path. The freestream velocity V_∞, assumed to be constant at 3.56 km/s, corresponds to freestream Mach number M_∞ of 12. The leading edge surface has a temperature T_w of 880 K for all cases considered. This temperature is chosen to be representative of the surface temperature near the stagnation point and is assumed to be uniform over the bodies.

Table 1: Freestream Conditions

T_∞ (K)	p_∞ (N/m^2)	ρ_∞ (kg/m^3)	n_∞ (m^{-3})	μ_∞ (Ns/m^2)	λ_∞ (m)	V_∞ (m/s)
220.0	5.582	8.753 x 10^{-5}	1.8209 x 10^{21}	1.455 x 10^{-5}	9.03 x 10^{-4}	3560

By assuming the nose diameter as the characteristic length, the overall Knudsen number Kn_D corresponds to 25, 5, 0.5, 0.25 and 0.09 for nose radius R_N/λ_∞ of 0.02, 0.1, 1, 2 and 5.5, respectively. The Reynolds number per unit of meter is $Re_\infty = 21416.3$, also based on conditions in the undistorted stream. The DSMC calculations were performed independently for three distinct numerical values for α_n and σ_t: 0.5, 0.75 and 1. It is important to mention that α_n and σ_t equal to 1 represent the diffusion reflection case.

5. Computational Results and Discussion

The aerodynamic performance of the round leading edges is assessed by using the heat transfer rate, the total drag and the shock wave standoff distance. In this way, the purpose of this section is to discuss differences in these properties due to variations on the surface accommodation coefficient of these bodies with different nose radius.

5.1. Heat Transfer Coefficient

Energy may be added to or subtracted from the body surface by three distinct processes: (1) molecular energy transport to and from the body surface, (2) radiant energy transport to and from the body surface, and (3) energy added to or removed from the surface by processes occurring within the body. By considering process (1), the heat flux q_w to the body surface is calculated by the net energy flux of the molecules impinging on the surface. The net heat flux q_w is related to the sum of the translational, rotational and vibrational energies of both incident and reflected molecules. A flux is regarded as positive if it is directed toward the surface. The heat flux q_w is normalized by the freestream kinetic energy flux $\frac{1}{2}\rho_\infty V_\infty^3$ and presented in terms of heat transfer coefficient C_h.

Distributions of the heat transfer coefficient C_h along the round leading edge surface are illustrated in Figs. 2(a-c) with the accommodation coefficient as a parameter. Figures 2(a-c) correspond to the dimensionless nose radius R_N/λ_∞ of 0.02, 1 and 5.5, respectively. In this set of figures, S is the arc length s normalized by the freestream mean free path λ_∞ measured from the stagnation point. The heat transfer coefficient C_h for R_N/λ_∞ of 0.1 and 2 is intermediate to those

shown in Figs. 2(a-c), therefore they will not be presented.

It is apparent from Figs. 2(a-c) that the heat transfer coefficient is sensitive not only to the normal and tangential accommodation coefficients but also to the nose radius. In general, C_h presents the maximum value in the stagnation point and drops off sharply along the cylindrically blunt portion up to the cylinder/wedge junction. It is noted from this set of figures that C_h decreases by a reduction in the normal accommodation coefficient and it increases with reducing the tangential accommodation coefficient. Moreover, either the normal or tangential accommodation coefficient affects the leading edges in a different way as the nose radius R_N/λ_∞ is reduced from 5.5 to 0.02. In addition to that, C_h at the stagnation region decreases with increasing the nose radius. This behavior seems to be in agreement with the continuum predictions for blunt body in that the heat flux scales inversely with the square root of the nose radius. As expected, by reducing the nose radius the leading edge becomes sharper and approaches the wedge leading edge as shown in Fig. 1(a).
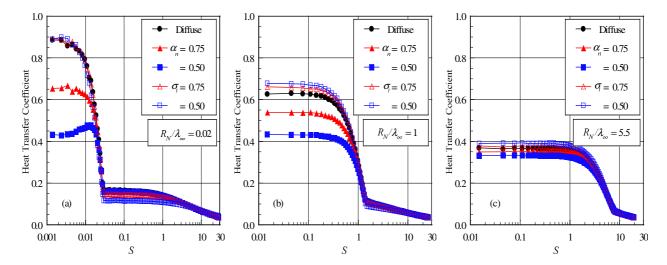

Figure 2: Distributions of the heat transfer coefficient C_h along the body surface as a function of the accommodation coefficient for round leading edges with R_N/λ_∞ (a) 0.02, (b) 1 and (c) 5.5.
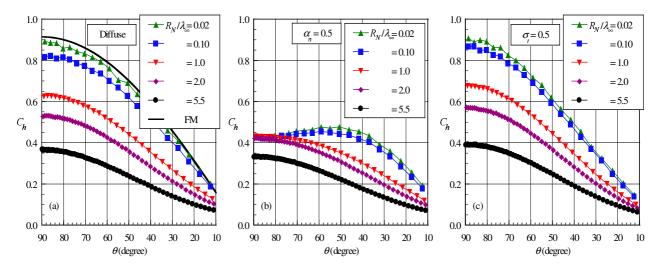

Figure 3: Distributions of the heat transfer coefficient C_h along the cylindrically portion of the round leading edges by considering (a) diffuse reflection, (b) α_n of 0.5 and (c) σ_t of 0.5.

Effects of both the incomplete surface accommodation and the nose radius on the heat transfer coefficient C_h can also be seen in a different way by displaying the results as a function of the body slope angle θ. Figures 3(a-c) depict C_h on the cylindrically portion of the leading edges as a function of the body slope angle for diffuse case, α_n of 0.5 and σ_t of 0.5, respectively. For comparison purpose, Fig. 3(a) presents C_h by assuming free molecular (FM) flow (Bird, 1994). Referring to Fig. 3(a), it is noted that C_h approaches the free molecular limit ($C_{ho} = 0.915$) in the cylindrically portion of the round leading edge with reducing the nose radius. It is clearly seen in Figs. 3(a-c) that C_h profiles are preserved for the majority of the cases investigated. In general C_h presents the maximum value at the stagnation region and decreases along the cylindrically portion of the leading edges. However, for cases with R_N/λ_∞ of 0.02 and 0.1 and α_n of 0.5 (see

Fig. 3(b)), the maximum point moves from the stagnation point, which corresponds to station $\theta = 90$ degree, to station around $\theta = 50$ degree.

The heat transfer coefficient at the stagnation point C_{ho} is displayed in Tab. 2 for the range of nose radius investigated. These values were obtained by a curve fitting process performed over the curves shown in Figs. 3(a-c).

Table 2: Heat transfer coefficient at the stagnation point C_{ho} for round leading edges.

R_N/λ_∞	0.02	0.1	1	2	5.5
Diffuse	0.883	0.824	0.630	0.532	0.366
$\alpha_n = 0.75$	0.660	0.622	0.537	0.484	0.352
$\alpha_n = 0.50$	0.436	0.433	0.429	0.424	0.333
$\sigma_t = 0.75$	0.894	0.859	0.660	0.553	0.377
$\sigma_t = 0.50$	0.904	0.868	0.676	0.571	0.391

5.2. Total Drag Coefficient

The drag on a surface in a gas flow results from the interchange of momentum between the surface and the molecules colliding with the surface. The total drag is obtained by the integration of the pressure p_w and shear stress τ_w distributions along the body surface. In this connection, p_w and τ_w distributions were considered from the nose of the leading edge to the station L, which corresponds to the tangent point common to all of the body shapes. The total drag presented in this section was obtained by assuming the shapes acting as leading edges. As a result, no base pressure effects were taken into account on the calculations. Before presenting the results for the total drag coefficient acting on the round leading edges, it proves helpful to visualize the manner in which the two accommodation coefficients as well as the nose radius affect pressure p_w and shear stress τ_w distributions along the body surfaces.

The influence on wall pressure due to variations on the nose radius and on the surface accommodation coefficient is demonstrated in Figs. 4(a-c) in terms of the pressure coefficient C_p defined by $(p_w - p_\infty)/\frac{1}{2}\rho_\infty V_\infty^2$. Figures 4(a-c) display the pressure coefficient C_p along the body surface for nose radius R_N/λ_∞ of 0.02, 1, and 5.5, respectively.

According to Figs. 4(a-c), it is seen that the pressure coefficient C_p follows the same trend as that presented by the heat transfer coefficient in that it presents the maximum value at the stagnation point and decreases fast in the cylindrically blunt portion of the leading edge. It is also verified that the pressure coefficient C_p in the cylindrically blunt portion is one order of magnitude higher than C_p in the wedge portion of the leading edge. At one hand, Figs. 4(a-c) demonstrate that the pressure coefficient C_p increases significantly at the vicinity of the stagnation point for sharp leading edges with reducing the normal accommodation coefficient. On the other hand, no appreciable changes are observed for those leading edges representing blunt leading edges. Consequently, the pressure coefficient C_p is a sensitive function of the nose radius when the normal accommodation coefficient is reduced from 1 to 0.5. One possible reason for this higher surface pressure might be that the molecules that are reflected upstream have a high kinetic energy with the partial accommodation model and, thus, when they recollide with the surface, they will impart a greater normal moment transfer. Moreover, it may also be recognized from Figs. 4(a-c) that the pressure coefficient C_p is insensitive to changes in the tangential accommodation coefficient.

Figures 5(a-c) illustrate the shear stress along the body surface in terms of the skin friction coefficient C_f, defined by $\tau_w/\frac{1}{2}\rho_\infty V_\infty^2$, for varying the nose radius and the normal and tangential accommodation coefficients. According to this set of figures, the skin friction coefficient C_f increases from zero at the stagnation point to a maximum that is still located in the cylindrically blunt portion of the leading edges, and decreases downstream along the body surface. It is also seen that the skin friction coefficient C_f presents an opposite behavior from that of pressure coefficient in the sense that it decreases with reducing the tangential accommodation coefficient. Furthermore, no changes are observed in the skin friction coefficient C_f for a reduction on the normal accommodation coefficient from 1 to 0.5. Also of great significance are the skin friction changes on the afterbody surface with diminishing the tangential accommodation coefficient, in contrast to the pressure coefficient behavior.

In what follows, it becomes instructive to present the results for the total drag obtained by the integration of the pressure p_w and shear stress τ_w distributions along the body surface. The DSMC results for total drag are normalized by $\frac{1}{2}\rho_\infty V_\infty^2 H$, where H is the height at the matching point common to the leading edges (see Fig. 1(a)), and presented as total drag coefficient C_d and its components of pressure drag C_{pd} and skin friction drag C_{fd} coefficients.

The impact of partial accommodation coefficient on the total drag coefficient C_d is demonstrated in Figs. 6(a-c) for nose radius R_N/λ_∞ of 0.02, 1 and 5.5, respectively. It is seen that as the leading edge becomes flatter the contribution of the pressure drag C_{pd} to the total drag C_d increases and the contribution of the skin friction drag C_{fd} decreases. For the sharpest round shape investigated, nose radius R_N/λ_∞ of 0.02, the major contribution to the total drag C_d is attributed to the skin friction coefficient, a characteristic observed in sharp leading edges. In contrast, for the bluntest case, nose radius R_N/λ_∞ of 5.5, the major contribution to the total drag C_d is attributed to the pressure coefficient, a blunt leading edge characteristic.
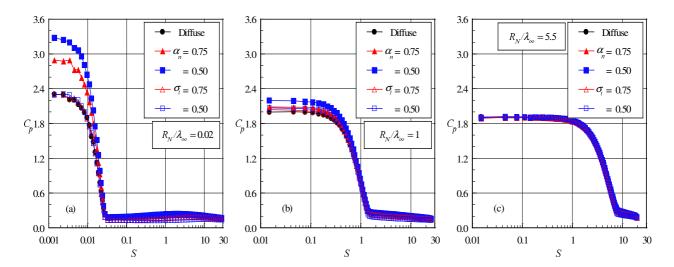
Figure 4: Distributions of pressure coefficient C_p along the body surface as a function of the accommodation coefficient for round leading edges with R_N/λ_∞ (a) 0.02, (b) 1 and (c) 5.5.
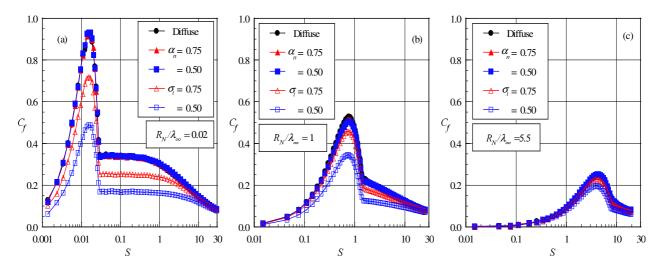

Figure 5: Distributions of skin friction coefficient C_d along the body surface as a function of the accommodation coefficient for round leading edges with R_N/λ_∞ (a) 0.02, (b) 1 and (c) 5.5.
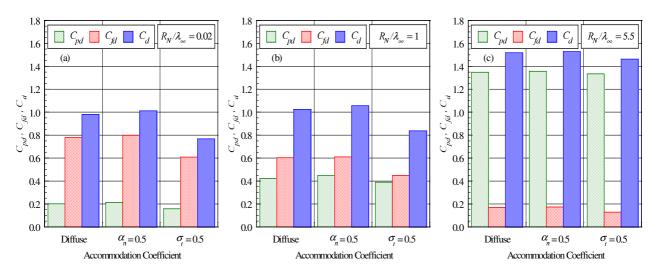

Figure 6: Pressure drag C_{pd}, skin friction drag C_{fd} and total drag coefficient C_d as a function of the accommodation coefficient for round leading edges with R_N/λ_∞ (a) 0.02, (b) 1 and (c) 5.5.

The effect of changing independently the normal and tangential accommodation coefficients on the total drag coefficient C_d for the round leading edges investigated is tabulated in Tab. 3. Referring to Tab. 3, it can be seen that variations in α_n or σ_t have a different effect on the total drag coefficient. The total drag coefficient C_d increases around 2% or 3% by a reduction in the normal accommodation coefficient, and decreases substantially by a reduction in the tangential accommodation coefficient for the leading edge shapes investigated. At this point, it should be emphasized that the total drag coefficient C_d for round leading edges approaches the wedge drag with decreasing the nose radius, as would be expected.

Table 3: Total Drag coefficient C_d for round leading edges.

R_N/λ_∞	0.02	0.1	1	2	5.5
Diffuse	0.978	0.979	1.028	1.085	1.519
$\alpha_n = 0.75$	0.994	0.995	1.039	1.144	1.523
$\alpha_n = 0.50$	1.011	1.012	1.057	1.158	1.528
$\sigma_t = 0.75$	0.908	0.910	0.957	1.074	1.496
$\sigma_t = 0.50$	0.766	0.767	0.837	0.975	1.462

5.3. Shock Wave Standoff Distance

The problem of predicting the shape and location of detached shock waves has been stimulated by the necessity for blunt noses and leading edges configurations designed for hypersonic flight in order to cope with the aerodynamic heating.

In a rarefied flow, the shock wave has a finite region that depends on the transport properties of the gas, and can no longer be considered as a discontinuity obeying the classical Rankine-Hugoniot relations. In this context, the shock standoff distance is defined as being the distance between the shock wave center and the nose of the leading edge along the stagnation streamline.

In order to quantify the shock standoff distance, the shock wave center is determined by employing the following procedure (Santos, 2004): the flow is assumed to consist of three distinct classes of molecules; those molecules from the freestream that have not been affected by the presence of the leading edge are denoted as class I molecules; those molecules that, at some time in their past history, have struck and been reflected from the body surface are denoted as class II molecules; and those molecules that have been indirectly affected by the presence of the body are defined as class III molecules. It is assumed that the class I molecule changes to class III molecule when it collides with class II or class III molecule. Class I or class III molecule is progressively transformed into class II molecule when it interacts with the body surface. Also, a class II molecule remains class II regardless of subsequent collisions and interactions. Hence, the transition from class I molecules to class III molecules may represent the shock wave, and the transition from class III to class II defines the boundary layer.

For illustration purpose, the distribution of molecules for each class along the stagnation streamline associated to sharp and blunt leading edges are demonstrated in Figs. 7 and 8, respectively. The impact of the surface accommodation on class I, II and II, related to round leading edge with R_N/λ_∞ of 0.02 is demonstrated in Figs. 7(a-c) for diffuse case, α_n of 0.5 and σ_t of 0.5, respectively. Similarly, Figs. 8(a-c) display the partial accommodation coefficient for round leading edge with R_N/λ_∞ of 5.5, the bluntest round leading edge investigated. In this set of figures, X is the distance x along the stagnation streamline, normalized by λ_∞, and f_I, f_{II} and f_{III} are the number of molecules for classes, I, II and III, respectively, to the total amount of molecules inside each cell. Based on these diagrams, the shock wave standoff distance Δ is defined as being the distance along the stagnation streamline from the shock wave center, position corresponding to the maximum value for f_{III}, to the nose of the leading edge.

By examining Figs. 7 and 8, it is clearly seen that there is a discrete shock standoff distance for the cases shown. It is also seen that partial accommodation coefficient affects the shock wave standoff distance along the stagnation streamline provided the leading edge is aerodynamically sharp. In contrast, no appreciable changes are observed for the bluntest case investigated, as either the normal or tangential accommodation coefficient is reduced from 1 to 0.5. The impact of changing independently the normal and tangential accommodation coefficients on the shock wave standoff distance Δ/λ_∞ for the round leading edges investigated is illustrated in Figs. 9(a,b).

According to Figs. 9(a,b), there is a discrete shock standoff distance for the round leading edge cases investigated. Furthermore, the shock standoff distance decreases with diminishing the nose radius. This is an expected result since shock standoff distance on a cylinder scales with the curvature radius. As a reference, the bluntest leading edges presents values for Δ/λ_∞ that are one order of magnitude larger than that for the sharpest leading edge investigated.

It is worthwhile to mention that the displacement of the shock wave is especially undesirable in a waverider geometry, because this hypersonic configuration usually depends on shock wave attachment at the leading edge to achieve its high lift-to-drag ratio at high-lift coefficient. Shock wave detachment will allow pressure leakage from the lower surface of the vehicle to the upper surface, thereby degrading the aerodynamic performance of the vehicle.
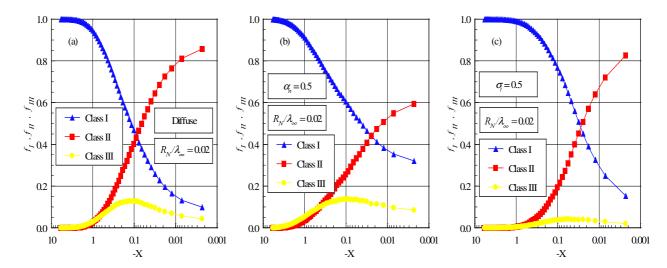
Figure 7: Distributions of molecules for classes I, II and III along the stagnation streamline for the round leading edge case with R_N/λ_∞ of 0.02: (a) diffuse, (b) α_n of 0.5 and (c) σ_t of 0.5.
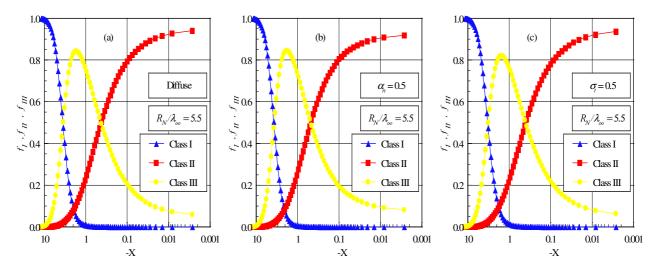

Figure 8: Distributions of molecules for classes I, II and III along the stagnation streamline for the leading edge case with R_N/λ_∞ of 5.5: (a) diffuse, (b) α_n of 0.5 and (c) σ_t of 0.5.
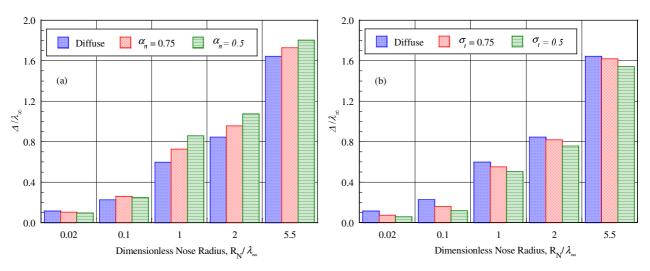

Figure 9: Dimensionless shock wave standoff distance Δ/λ_∞ along the stagnation streamline for round leading edges with (a) normal and (b) tangential accommodation coefficients of 0.5, 0.75 and 1.

6. Concluding Remarks

Direct Simulation Monte Carlo method is applied to examine rarefied gas over a group of round leading edges. Effects of incomplete surface accommodation on the heat transfer, total drag and shock wave standoff distance for a representative range of normal and tangential accommodation coefficients are investigated. The normal and tangential accommodation coefficients are varied from 1.0 to 0.5. Cases considered in this study cover the hypersonic flow on the transition flow regime.

Calculations showed that a reduction in the normal accommodation coefficient from 1.0 to 0.5 decreased the heat transfer coefficient in the vicinity of the stagnation point for the round shapes investigated. In contrast, a reduction in the tangential accommodation coefficient increased slightly the heat transfer coefficient near the nose of the leading edges. Also, it was found that the total drag coefficient is reduced by a reduction in the tangential accommodation coefficient, and increased by a reduction in the normal accommodation coefficient.

The analysis also showed that shock standoff distance are sensitive to changes on the surface accommodation coefficient. In general, it was observed that shock wave standoff distance decreased by a reduction on the tangential accommodation coefficient and increased by reducing the normal accommodation coefficient.

The effects of either normal or tangential accommodation coefficient showed that in order to make accurate predictions of the aerodynamic forces on, and heat transfer rates to, bodies in rarefied hypersonic flow it will be necessary to take surface accommodation into account.

7. References

Bird, G. A., 1981, "Monte Carlo Simulation in an Engineering Context", Progress in Astronautics and Aeronautics: Rarefied gas Dynamics, Ed. Sam S. Fisher, Vol. 74, part I, AIAA New York, pp. 239-255.

Bird, G. A., 1989, "Perception of Numerical Method in Rarefied Gasdynamics", Rarefied gas Dynamics: Theoretical and Computational Techniques, Eds. E. P. Muntz, and D. P. Weaver and D. H. Capbell, Vol. 118, Progress in Astronautics and Aeronautics, AIAA, New York, pp. 374-395.

Bird, G. A., 1994, "Molecular Gas Dynamics and the Direct Simulation of Gas Flows", Oxford University Press, Oxford, England, UK.

Borgnakke, C. and Larsen, P. S., 1975, "Statistical Collision Model for Monte Carlo Simulation of Polyatomic Gas Mixture", Journal of computational Physics, Vol. 18, No. 4, pp. 405-420.

Lord, R. G., 1991, "Application of the Cercignani-Lampis Scattering Kernel to Direct Simulation Monte Carlo Method", Proceedings of the 17th International Symposium on Rarefied Gas Dynamics, edited by A. E. Beylich, Aachen, Germany, pp. 1427-1433, July 8-14.

Santos, W. F. N., 2004, "Numerical Prediction of Stagnation-Point Shock-Detachment Distance for Hypersonic Low-Density Flow over Blunt Nose Shapes", Proceedings of the 24th International Congress of the Aeronautical Sciences, ICAS 2004, 29 Aug – 3 Sept, Yokohama, Japan.

Shvets, A. I., Voronin, V. I., Blankson, I. M., Khikine, V. And Thomas, L., 2005, "On Waverider Performance with Hypersonic Flight Speed and High Altitudes", 43rd AIAA Aerospace Sciences Meeting and Exhibit, AIAA Paper 2005-0512, Reno, NV.